Vessel maturation schedule determines vulnerability to neuronal injuries of prematurity

Tamar Licht,[1] Talia Dor-Wollman,[2] Ayal Ben-Zvi,[1,3] Gadiel Rothe,[1] and Eli Keshet[1]

[1]Department of Developmental Biology and Cancer Research, Hebrew University of Jerusalem, Jerusalem, Israel. [2]Neuropediatric Unit, Hadassah–Hebrew University Medical Center, Jerusalem, Israel. [3]Department of Neurobiology, Harvard Medical School, Boston, Massachusetts, USA.

Premature birth is a major risk factor for multiple brain pathologies, notably periventricular leukomalacia (PVL), which is distinguished by bilateral necrosis of neural tissue around the ventricles and a sequela of neurological disturbances. The 2 hallmarks of brain pathologies of prematurity are a restricted gestational window of vulnerability and confinement of injury to a specific cerebral region. Here, we examined the proposition that both of these features are determined by the state of blood vessel immaturity. We developed a murine genetic model that allows for inducible and reversible VEGF blockade during brain development. Using this system, we determined that cerebral vessels mature in a centrifugal, wave-like fashion that results in sequential acquisition of a functional blood-brain barrier and exit from a VEGF-dependent phase, with periventricular vessels being the last to mature. This developmental program permitted selective ablation of periventricular vessels via episodic VEGF blockade within a specific, vulnerable gestational window. Enforced collapse of ganglionic eminence vessels and resultant periventricular neural apoptosis resulted in a PVL-like phenotype that recapitulates the primary periventricular lesion, ventricular enlargement, and the secondary cortical deficit in out-migrating GABAergic inhibitory interneurons. These findings provide an animal model that reproduces the temporal and spatial specificities of PVL and indicate that damage to VEGF-dependent, immature periventricular vessels contributes to PVL development.

Introduction

Premature birth is a major risk factor for a number of CNS pathologies that, with the sharp increase in survival of infants with a very low birth weight (VLBW, ≤ 1500 g), pose an ever-increasing medical burden. Of particular significance are the blindness-causing disease retinopathy of prematurity (ROP) and periventricular leukomalacia (PVL). The latter is an encephalopathy of prematurity developing in up to 50% of VLBW infants and associated with cognitive and behavioral deficits in 25% to 50% of cases and with major motor deficits (e.g., cerebral palsy) in 5% to 10% of cases (for a recent review on PVL, see ref. 1 and references therein).

Common to both diseases is a precipitous drop in disease incidence at late gestational ages and full refractoriness at term. It is generally believed that this temporal pattern reflects a gestational age–restricted vulnerability window to some insult, possibly an iatrogenic insult associated with management of the immature infant. In the case of ROP, it was indeed shown that ventilation therapy (i.e., exposure to hyperoxia) leads to obliteration of retinal vessels and a resultant retinal hypoxia, triggering, in turn, an excessive angiogenic response and culminating in preretinal growth of leaky vessels, a process faithfully reproduced in the widely used oxygen-induced retinopathy (OIR) mouse model (2).

▶ Related Article: p. 965

Authorship note: Tamar Licht and Talia Dor-Wollman contributed equally to this work.
Conflict of interest: The authors have declared that no conflict of interest exists.
Submitted: October 7, 2014; **Accepted:** January 2, 2015.
Reference information: *J Clin Invest*. 2015;125(3):1319–1328. doi:10.1172/JCI79401.

Further mechanistic insights on ROP pathogenesis were obtained using the OIR model and showing that placing newborn mouse pups in a hyperoxic incubator suppresses production of the oxygen-regulated factor VEGF beyond the critical level required to sustain immature retinal vessels (and newly formed, immature vessels only) and, consequently, induces their selective obliteration and development of an ROP-like pathology. Importantly, mice turned fully refractory to this insult upon maturation of retinal vessels at later stages, thus implicating vessel maturation as the critical event marking a closure of the vulnerability window (3). These findings raise the question of whether a similar pathogenic mechanism may also apply to diseases affecting the brain of VLBW immature infants, such as PVL.

PVL is a distinctive form of cerebral white-matter injury characterized by either focal or diffuse necrotic lesions preferentially distributed near the lateral ventricles and by complex sequelae of destructive and developmental disturbances in a constellation generally described as encephalopathy of prematurity (4). The underlying cause of PVL, particularly what triggers its upstream event of periventricular neuronal death, is not well understood. One proposed mechanism links PVL to an inflammatory response to intrauterine infection (5–7), while another proposed mechanism for PVL pathogenesis ascribes neuronal damage to local cerebral ischemia and reduced perfusion of the germinal matrix (GM), a region nourished by a dense network of blood vessels and rich in proliferating neural and glial progenitors (4, 8, 9). Yet neither of these proposed etiologies provides a satisfactory explanation for the 2 major questions regarding PVL, namely, why initial neuronal damage is confined to the periventricular region and why premature infants who have passed

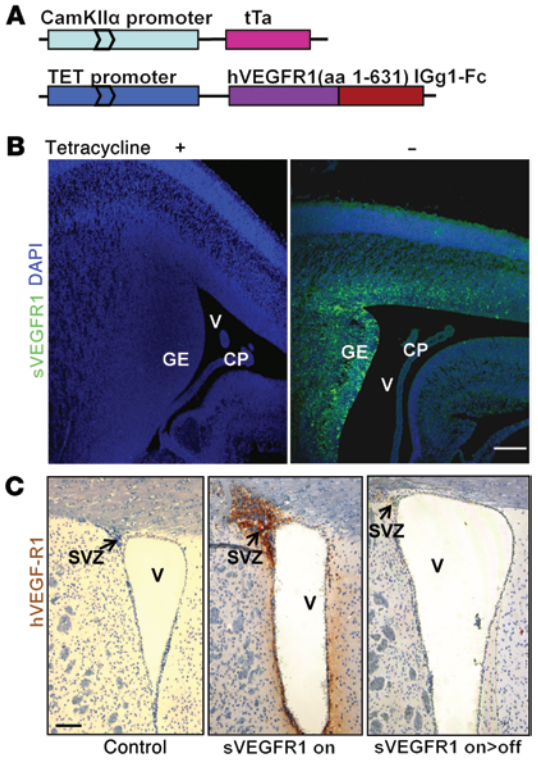

Figure 1. A system for brain-specific, conditional VEGF LOF. (**A**) A schematic of the "driving" CamkIIα-tTA transgene and the "responder" tetracycline-regulated sVEGFR1 transgene composing the conditionally induced bitransgenic system. (**B**) Immunostaining of sagittal E16.5 embryo sections for human VEGFR1 (not detecting endogenous receptor variants) in the presence ("off" mode) or absence ("on" mode) of tetracycline. (**C**) Immunostaining of adult (6 months old) brain sections for hVEGFR1 maintained in the off mode (left), on mode (middle), or an on/off mode (right). Note full reversibility of transgene induction. Images were reproduced 6 times. Scale bars: 100 μm. V, lateral ventricle; CP, choroid plexus.

a critical gestation age are no longer vulnerable. Addressing these 2 fundamental issues has been hampered by the lack of an appropriate animal model capable of reproducing any of these disease hallmarks.

On the premise of a vascular basis for PVL pathogenesis, we herein propose that immature blood vessels in the developing brain are the primary target of PVL-inducing insults. Correspondingly, we argue that the unique temporal and spatial patterns of the disease are determined by the developmentally programmed pattern of cerebral vessel maturation. A critical examination of this proposition first necessitated elucidating spatial and temporal patterns of vascular maturation in the developing brain. Two functional features distinguishing mature from immature vessels are the acquisition of a functional blood-brain barrier (BBB) and the acquisition of VEGF-independent status, with the latter bearing a particular relevance to insults associated with perturbations in brain oxygenation. Using both parameters, a developmentally programmed inward wave of vessel maturation was uncovered in which periventricular vessels were the last among all cerebral vessels to mature and hence the only vessels still dependent on VEGF at the time of premature birth.

Because management of VLBW newborns almost always involves high oxygen treatment, it could be hypothesized that PVL also shares with ROP a seemingly paradoxical situation in which excessive oxygen, because it leads to obliteration of immature vessels, counterintuitively produces the proximal insult of insufficient oxygen. Consistent with this proposition are studies in prematurely delivered baboon neonates showing that the mode of ventilatory support greatly affects the severity of PVL-like cerebral damage (10, 11). Notably, vascular imaging in human PVL infants has revealed a defect of periventricular vessels in the deep white matter, with a pattern indicative of their physical loss at this site (8) reminiscent of the focal vascular loss typifying ROP. Together, these findings have provided us with a rationale for examining whether VEGF loss of function (LOF), as anticipated under circumstances of oxygen imbalance, might play a role in PVL pathogenesis.

Here, we show that even a short episode of VEGF blockade, provided that it takes place during the vulnerable time window but not later, is sufficient to produce a PVL-like periventricular lesion as well as a PVL-like permanent deficit in late out-migrating interneurons.

Results

A genetic system for inducible and reversible VEGF blockade at successive stages of brain development. To allow for conditional and reversible VEGF LOF at defined developmental timings, a bitransgenic mouse system based on conditional induction (and, in turn, deinduction) of a secreted VEGF decoy receptor was developed and used throughout the study. Briefly, a transgenic mouse expressing a secreted chimeric protein composed of the VEGF-binding domain of VEGFR1 fused to an IgG1-Fc tail and driven by a tetracycline-inducible promoter (Tet-sVEGFR1 "responder" line) (12) was crossed with a transgenic mouse expressing a tetracycline-dependent transactivator protein (tTA) driven by a brain-specific calmodulin kinase IIα promoter (CamkIIα-tTA "driver" line) (13). The VEGF decoy receptor is specifically induced in the brain of CamkIIα-tTA::TET-sVEGFR1 double-transgenic mice within 24 hours of withdrawing tetracycline from the drinking water (Tet-off), sequestering VEGF and precluding signaling (see schematic in Figure 1A and Methods for details).

The CamkIIα promoter was chosen as the driving promoter due to its activity in the developing cortex encompassing the GM bordering the ventricles (Figure 1B), which is also the site of primary injury in PVL. Initial experiments have shown that the CamkIIα promoter drives efficient sVEGFR1 production in the GM at all developmental times (Supplemental Figure 1; supplemental material available online with this article; doi:10.1172/JCI79401DS1) and in the subventricular zone (SVZ) and around the ventricles up to adulthood (Figure 1C and ref. 14). It is noteworthy that, because it is a secreted protein, induced sVEGFR1 is also accessible to cortical layers extending beyond its site of production. Resuming tetracycline addition (on-off regime) led to rapid deinduction of sVEGFR1 (Figure 1C and corroborated by Northern blotting and ELISA for the soluble receptor; data not shown), thereby allowing transient VEGF blockade at all developmental intervals of choice.

Cerebral regions affected by VEGF LOF become progressively restricted as gestation progresses and eventually are confined to the periventricular ganglionic eminence zone. To determine the developmental timing and spatial distribution of acquiring VEGF refractoriness, sVEGFR1 was induced at sequential stages of brain development by omitting tetracycline from the drinking water of pregnant mothers, starting at

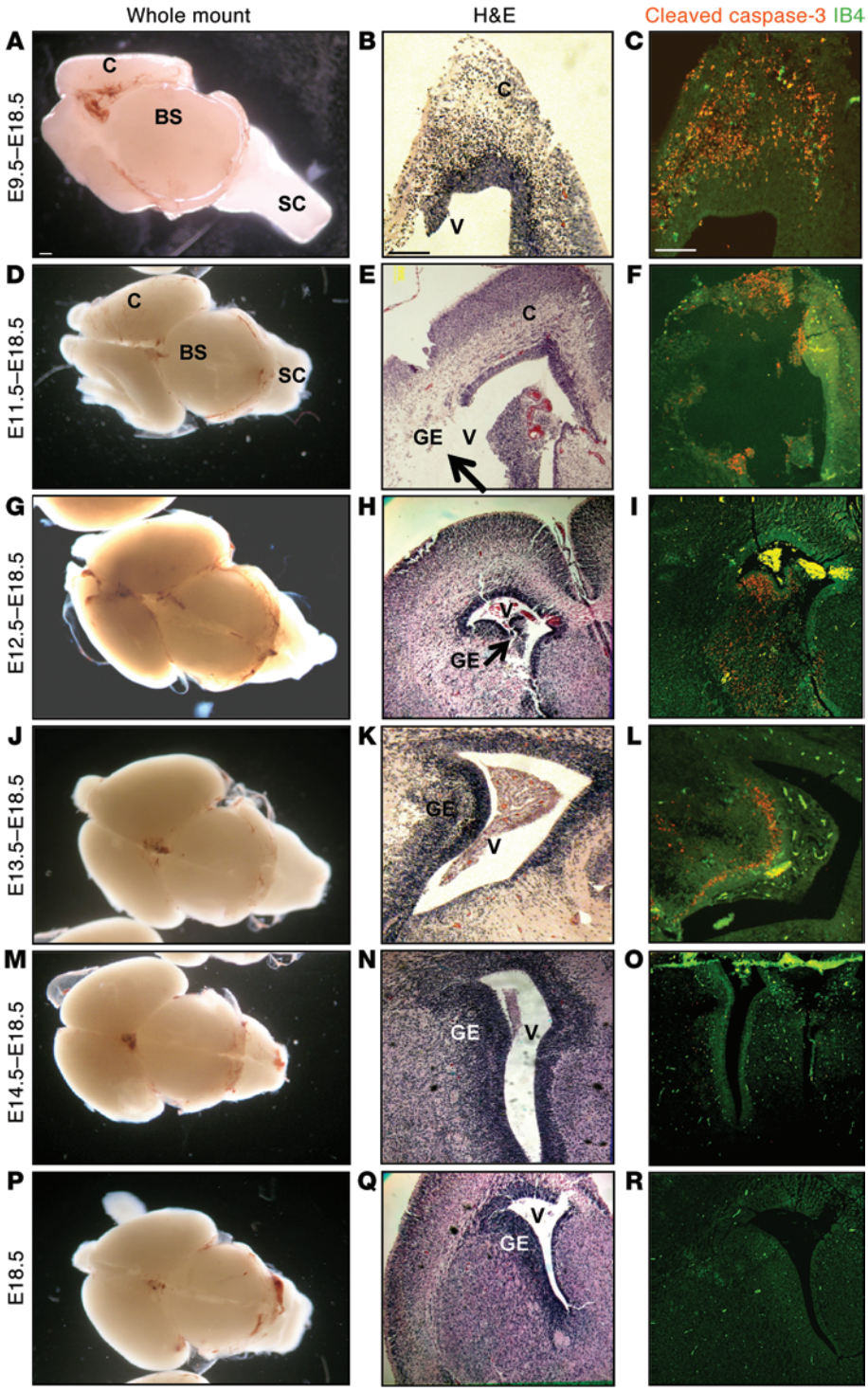

Figure 2. Spatiotemporal mapping of a developmental transition to a VEGF-refractory state. sVEGFR1 was induced at the indicated times of embryonic development, and all brains were retrieved for analysis at E18.5. For comparison, a nonmanipulated E18.5 brain is shown in the lower panels (**F**, **Q**, **R**). Left panels (**A**, **D**, **G**, **J**, **M**, **P**): whole brains; middle panels (**B**, **E**, **H**, **K**, **N**, **Q**): H&E-stained coronal sections at the level of the lateral ventricle and GM; right panels (**C**, **F**, **I**, **L**, **O**, **R**): adjacent serial sections stained for blood vessels (IB4) and for apoptosis (cleaved caspase-3). Note progressive reduction in regions undergoing apoptosis and complete resistance to VEGF knockdown from E14.5. Every age group was reproduced at least 3 times. C, cortex; BS, brain stem; SC, spinal cord. Arrows indicate areas of tissue necrosis. Scale bars: 200 μm.

E9.5. Initiating the VEGF blockade anytime earlier than E12.5 resulted in postpartum death, which was similar to the postpartum death phenotype observed in transgenic mice harboring brain-specific VEGF-insufficient alleles (15). Later onsets of VEGF blockade, from E12.5 and onwards, yielded viable pups surviving to adulthood.

Inspection of brains retrieved close to birth revealed that, while cortical size was dramatically reduced when sVEGFR1 was induced on E9.5, progressive diminution of cortical thinning was evident in brains in which VEGF blockade was initiated between E9.5 and E11.5 (Figure 2, A–F), and no cortical thinning was evident when it was initiated at E12.5 or later (Figure 2, G–R). In situ visualization of cells undergoing apoptosis revealed that, contrary to widespread apoptosis induced by VEGF blockade at early stages, apoptosis was progressively more restricted if initiated at later stages and from E13.5 was confined to only a few rows of cells lining the lateral wall of the lateral ventricle (Figure 2L; see also enlarged image in Figure 4E). Of note, this area encompasses the medial and lateral ganglionic eminence (GE), which is the functional equivalent of the human subpallial part of the GM. Remarkably, apoptosis was no longer detectable when the onset of VEGF blockade was delayed by only 1 day (Figure 2, M–O). These results thus point at the GE in the lateral wall as the last region to undergo transition from a VEGF-dependent to a VEGF-independent state and to the E13.5–E14.5 interval as the critical period when this transition takes place. Because it may take up to 1 day for tetracycline to be fully cleared and for sVEGFR1 to be induced, as is indeed demonstrated in Supplemental Figure 1, actual gestational stages affected by VEGF LOF might, in fact, be more than 1 day later than indicated. Levels of induced sVEGFR1 stayed high even after closure of the vulnerability window (Supplemental Figure 1), indicating that undetectable vessel regression reflects a genuine transition to a VEGF-refractory phase.

To rule out the possibility that preferential vulnerability of the GE is not merely a reflection of a preferential expression of the driving promoter at this site, we resorted to VEGF LOF using another, ubiquitous driving promoter. In these experiments, a Rosa26-rtTA driver mouse replaced the CamkIIα-tTA driver mouse for conditional

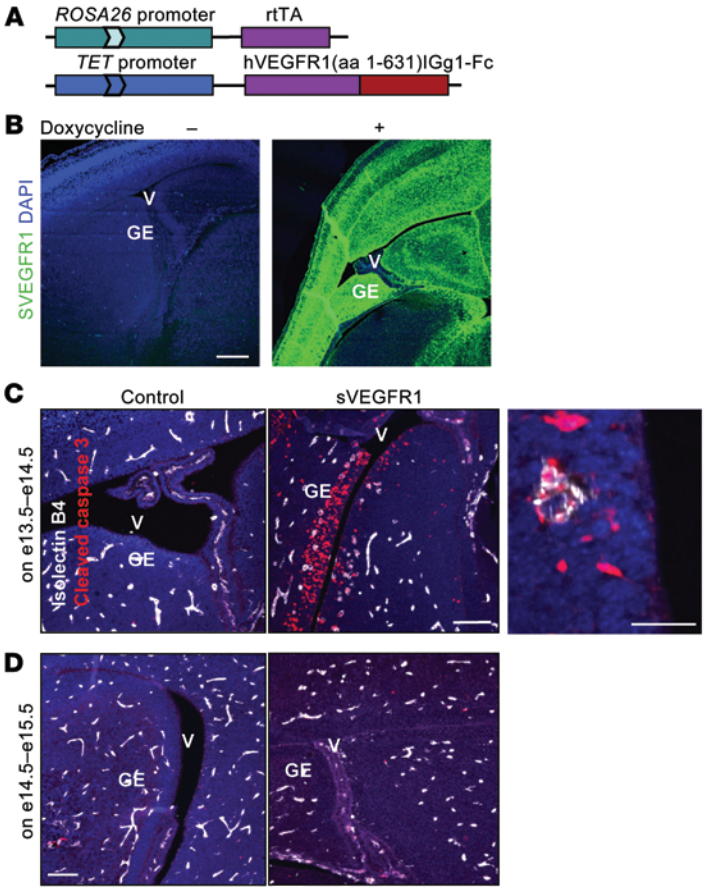

Figure 3. Cerebral apoptosis induced by global VEGF LOF with the aid of a rosa26-rtTa driver line. (**A**) Schematic of transgenic mouse lines used. (**B**) Immunostaining for hVEGFR1 in E15.5 brain induced 1 day earlier (noninduced littermate control on left). Note robust induction of the VEGF-trapping receptor throughout. Scale bar: 200 μm. (**C**) E14.5 brains in which sVEGFR1 was switched on 1 day earlier stained for blood vessels (IB4) and apoptosis (cleaved caspase-3) and highlighting GE-specific apoptosis, including EC apoptosis. Higher magnification is shown on right. Scale bars: 100 μm (left, middle); 20 μm (right). (**D**) E15.5 brain switched on 1 day earlier and showing no evidence for GE apoptosis. Scale bar: 100 μm. Image observations were reproduced 3 times.

sVEGFR1 induction (Figure 3A). In Rosa26-rtTA::TET-sVEGFR1 double-transgenic mice, sVEGFR1 was indeed efficiently induced upon doxycycline addition in all areas of the brain (Figure 3B) and elsewhere (not shown). Because global VEGF inhibition leads to embryonic lethality within a couple of days, it was only possible to switch on sVEGFR1 in this system for 1 day. Based on results shown above, we elected to switch on sVEGFR1 in the E13.5–E14.5 and the E14.5–E15.5 intervals, i.e., just prior to and immediately following anticipated transition of the GE to a VEGF-refractory stage. As shown in Figure 3C, VEGF blockade at the E13.5–E14.5 interval indeed resulted in massive apoptosis of both endothelial and nonendothelial cells residing in the ventricular wall, but not in more distantly located periventricular layers. Consistent with findings presented in Figure 2, 1 day later, the ventricular wall became fully refractory to VEGF withdrawal (Figure 3D), thereby corroborating both the regional and temporal specificities of periventricular vulnerability.

Vascular loss caused by VEGF blockade precedes neuronal apoptosis. VEGF blockade during critical stages of brain development leads to a distinct pattern of brain damage (characterized below). In order to determine whether neuronal damage is secondary to vascular injury or, alternatively, might be due to a direct effect of VEGF on nonendothelial cells, we first examined whether VEGF receptors are expressed on nonendothelial cells, focusing on the relevant area where neuronal damage is initially detected, namely the GE. The key VEGF-signaling receptor VEGFR2 (Flk1) was found to be exclusively expressed on endothelial cells in this region (Figure 4A) as well as in all other brain regions examined (not shown). A similar situation of endothelially restricted expression was also found for VEGFR1 (Flt1). Due to the very low level of VEGFR1 expression, however, undetectable by in situ immunofluorescence, we resorted to in situ RNA analysis in which a very low signal could be detected in endothelial cells but nowhere else (Figure 4B). Considering, however, previous reports on VEGFR2 expression in nonendothelial hippocampal cells (15), low-level expression of VEGF receptors in nonendothelial cells, below our detection levels, cannot be excluded. Consistent with the contention that neuronal damage due to VEGF LOF is not mediated by direct signaling to neurons are findings of Haigh et al. (16) showing that the severe neuronal damage usually observed following cerebral VEGF knockout could not be detected following a neuronal-specific knockout of Flk1.

To provide further support to the assertion that neuronal damage is secondary to vascular loss, we next determined whether endothelial and neuronal apoptosis occur concomitantly or sequentially. To this end, sVEGFR1 was induced at E13.5 and brains were examined 2 or 3 days thereafter. As shown in Figure 4C, 2 days of VEGF blockade were sufficient to obliterate GE vessels and, consequently, to generate focal GE hypoxia (visualized with the aid of the hypoxia marker Hypoxyprobe, Figure 4D). Yet no neuronal cell apoptosis could be detected at this time. Prolonging the VEGF blockade for 1 additional day, however, led to massive apoptosis of both neuronal and endothelial cells in the GE (Figure 4, E and F). The fact that endothelial apoptosis and resultant hypoxia precede neuronal apoptosis strongly argues that death of GE neurons is consequent to vascular loss.

Remarkably, endothelial cell apoptosis due to VEGF withdrawal resulted in complete clearance of blood vessels from the area and in the creation of an avascular zone. The avascular periventricular zone generated by VEGF blockade bears a striking resemblance to the focal pattern of avascularity observed in neonates with PVL, as visualized in a barium sulfate–perfused brain obtained postmortem from a neonate born prematurely and diagnosed with PVL (8). The area devoid of perfused blood vessels in the PVL patient is the same locale as the avascular zone generated by VEGF blockade.

Selective vulnerability of periventricular vessels is correlated with their delayed maturation and BBB closure. To gain insights regarding the cellular basis for the selective dependence of periventricular vessels on VEGF, we compared the developmental timing of pericyte recruitment to different cerebral vascular beds. This is because the acquisition of pericyte coverage was previously shown to mark vessel maturation with regard to distinguishing VEGF-

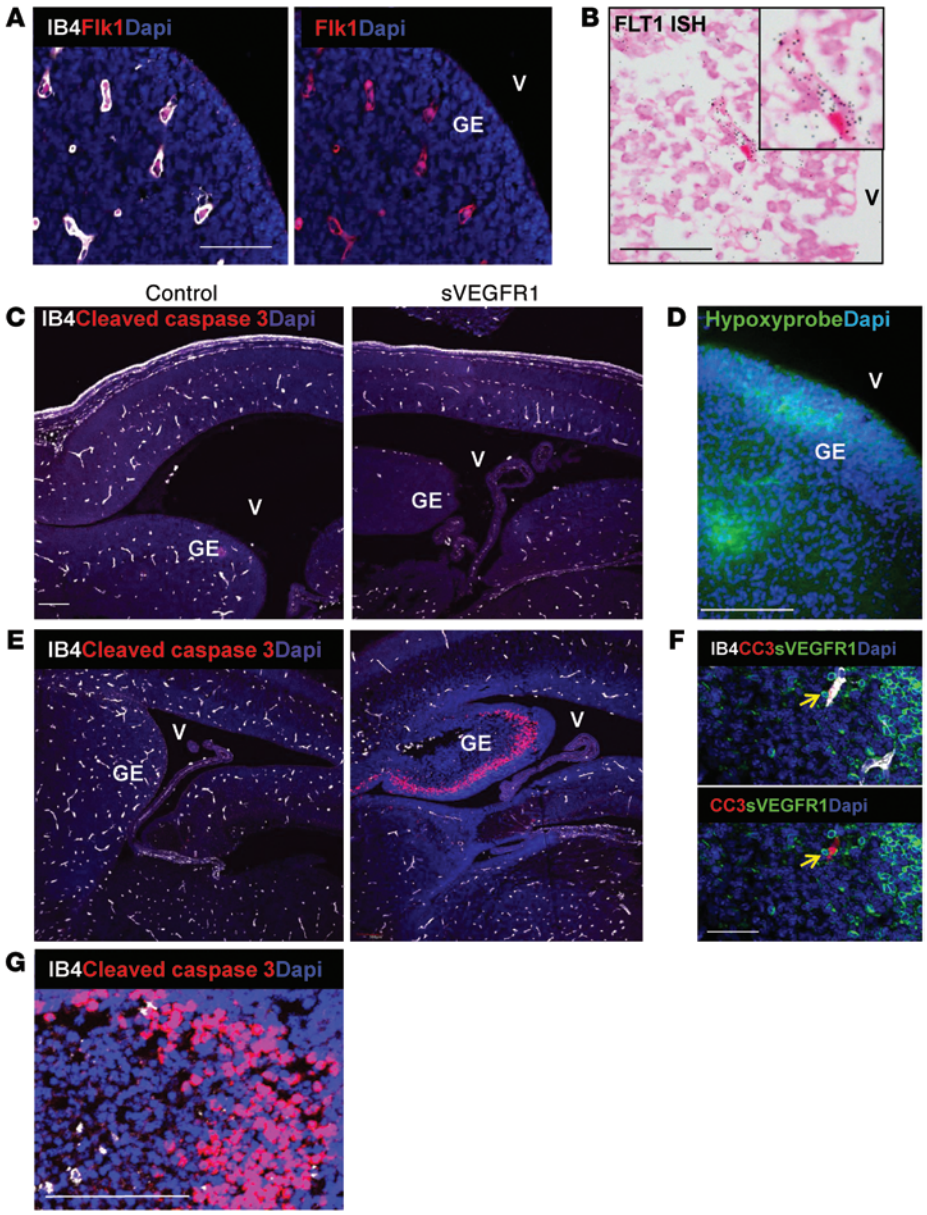

Figure 4. Vascular loss and hypoxia precede GE neuronal loss. (**A**) The VEGF receptor Flk1, illustrated by immunofluorescence, colocalizes with endothelial cells in the GE. (**B**) In situ hybridization for Flt1 shows higher grain density in a capillary encompassing erythrocytes. Scale bars: 50 μm (**A** and **B**). (**C**–**G**) sVEGFR1 was induced at E13.5, and brain was retrieved at E15.5 (**C**, **D**, and **F**) or at E16.5 (**E** and **G**) and stained for endothelial cells (IB4) and apoptosis (CC3) or for hypoxia (with Hypoxyprobe). Note that 2 days of VEGF blockade were sufficient to completely eliminate GE vessels and generate GE hypoxia (with occasional endothelial cell caught undergoing apoptosis, **F**), but with no evidence for GE neuronal apoptosis. The latter was, however, clearly evident after 1 additional day of VEGF blockade. Note at a higher magnification (**G**) that cells undergoing apoptosis are mostly nonvascular cells. Image observations were reproduced at least 4 times. Scale bar: 100 μm (**C**–**G**).

independent from VEGF-dependent vessels in the developing retina (17) and to play a role in BBB formation (18, 19). Results showed that the recruitment of NG2$^+$ pericytes to GE vessels indeed lagged behind their recruitment to cortical and other (e.g., to brain stem) vascular beds (Supplemental Figure 2A). Yet the process was nearly completed by E12.5, and therefore, mere physical engagement with NG2$^+$ pericytes could not explain the phenotypic switch of GE vessels to a VEGF-refractory state.

In the brain, BBB maturation of newly formed cerebral vessels is associated with the appearance of tight-junction molecules (20, 21). To determine whether periventricular vessels may acquire tight junctions later than other cerebral vessels, we first stained endothelial cells for the tight-junction molecules zona occludens-1 (ZO-1) and claudin-5, known to be essential for BBB function. Results indeed showed a graded increase in the fraction of endothelial cells expressing ZO-1 and claudin-5 and a delayed onset of their expression by GE vessels relative to their expression in other cortical regions or the brain stem (Supplemental Figure 2, B and C). The transition of GE vessels from claudin-5 negativity to claudin-5 positivity mostly took place between E13.5 and E15.5, i.e., coinciding with their transition to a VEGF-refractory stage.

In search of functional evidence that BBB acquisition by periventricular vessels lags behind that of other cerebral vessels, we used a newly developed methodology suitable for in utero measurements of BBB functionality (22). The method is based on intrahepatic injection of a fluorescent tracer (10 kDa TRITC-labeled dextran) and visualizing vascular leaks in sections of brain retrieved 5 minutes after injection (see Methods for details). Based on results shown above regarding developmental onset of BBB marker expression, we focused on the E14.5–E16.5 interval as the presumed relevant period for BBB consolidation in the periventricular region. At E14.5, GE vessels clearly had not yet sealed their barrier, as evidenced by a failure to contain the tracer within the lumen and its distribution in the parenchyma surrounding the vessels. At least some vessels residing in the dorsal ventricular zone (DVZ) seemed to already have better barrier function. Outer cortical vessels, such as in the ventral cortex, already had a functional barrier at this time (Figure 5A). At E14.5, all vessels were already perfused, as a large molecular tracer (500 kDa FITC-labeled dextran) was retained in the lumen (Supplemental Figure 3). By E15.5, all vessels in the periventricular and cortical areas had improved BBB function, evidenced by clear luminal entrapment of the tracer (Figure 5B). Full functionality was achieved at E16.5, evidenced by full containment of the tracer within vessels (Figure 5C). These results further substantiate a tight correlation between the acquisitions of a functional BBB and a transition to a VEGF-independent state and identify GE vessels as the last vessels to exit the vulnerability window.

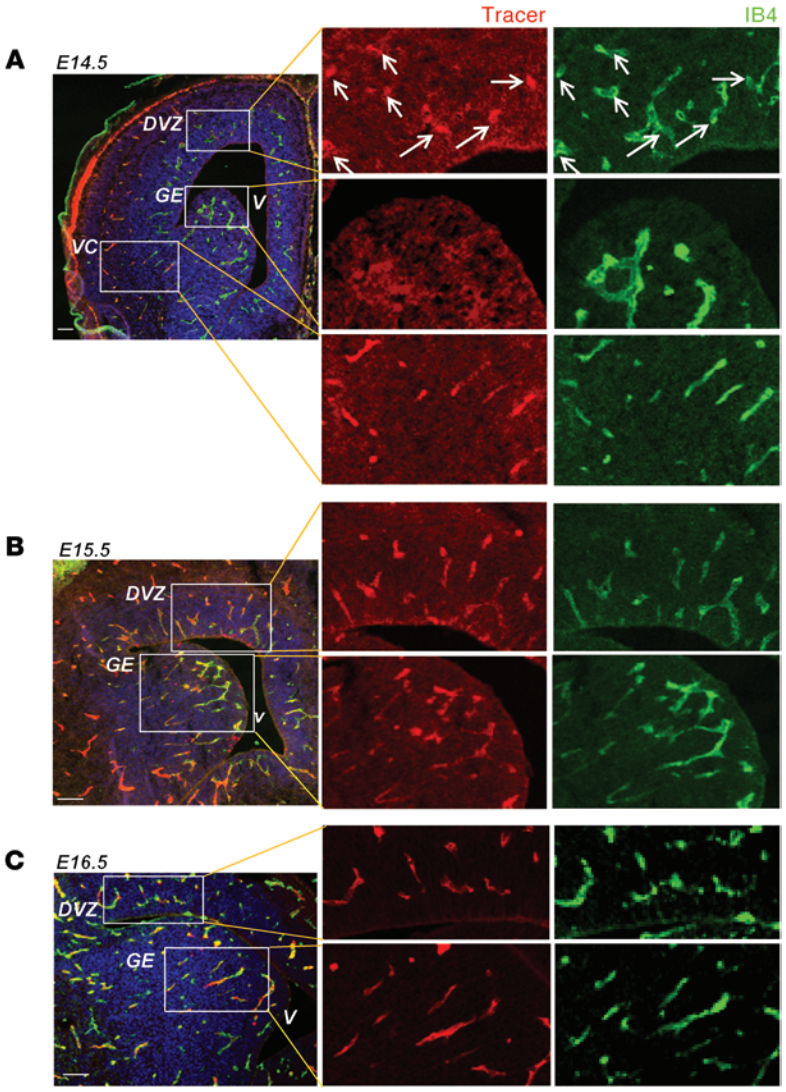

Figure 5. Delayed acquisition by GE vessels of a functional BBB. Leakage of intrahepatically injected fluorescent tracer in WT brains of E14.5 (**A**), E15.5 (**B**), and E16.5 (**C**) embryos was visualized in brain sections as described in Methods. Leakage is evident by a failure to contain the tracer (red) within vessels (vessels highlighted by IB4 staining in green) and a diffused parenchymal staining. Note BBB maturation of GE vessels while they transit from leaky vessels to a more sealed vessel state between E14.5 and E15.5. In the DVZ, at least some vessels seem to have already acquired some barrier function already at E14.5 (arrows), while in outer cortical areas such as the ventral cortex (VC) the BBB is sealed at E14.5. Images reproduced represent at least 3 embryos per age group. Scale bars: 100 μm.

Loss of periventricular vessels leads to a PVL-like phenotype: primary periventricular lesions. The myriad of PVL-associated lesions is generally divided into a primary component underlined by a loss of multiple cell types residing deep in periventricular white matter and secondary neuronal damage, primarily loss of neuronal subsets originating at and out-migrating from the affected GE. We, therefore, wished to determine whether VEGF blockade and a resultant collapse of periventricular vasculature would produce both components of the disease. To this end, sVEGFR1 was induced at E12.5–E13.5, and animals were inspected 20 to 30 days after birth. Manipulated mice showed a striking 30% reduction in body weight compared with littermate controls, indicative of significant systemic consequences of the inflicted brain injury (Figure 6A, left). The deficit in growth was, however, compensated with time.

Gross inspection of the overall smaller, olfactory bulb–deficient brain (Figure 6A, right, and ref. 14) revealed a dramatic enlargement of the lateral ventricle occupying the space of a largely reduced striatum. The marked reduction (about two-thirds) in striatal size was disproportionate to the apparently normal size of the cortex (Figure 6B). The SVZ was dramatically thinned to include only a few patches of proliferating cells (highlighted by Ki-67 staining) (Figure 6, C and D). This phenotype, namely, ventricular enlargement and reduced periventricular tissue, bears a striking resemblance to human PVL (see Supplemental Figure 4C). Notably, these abnormalities persisted at older ages and were also evident at 8 months of age (the latest age examined; data not shown).

Insults to the preterm infant can cause permanent brain damage even if lasting for a limited duration, provided that they take place during the vulnerability window (24–30 weeks of gestation). We therefore wished to determine whether a short, transient VEGF blockade exercised at the vulnerable time window would be sufficient to produce permanent brain damage similar to that inflicted by a continuous insult. To this end, sVEGFR1 was induced at E12.5 and deinduced at E15.5 (on-off switching mode); the brain was retrieved for analysis 20 days after birth. Efficient deinduction of sVEGFR1 was verified using both ELISA and immunohistochemistry for the extracellular domain of human VEGFR1 (not shown). Limiting VEGF blockade to the E12.5–E15.5 interval reproduced the brain abnormalities observed in mice in which sVEGFR1 was continuously "on" from E12.5 onwards. Specifically, body weight was similarly reduced (not shown), ventricles were enlarged, and the striatum was similarly reduced (Supplemental Figure 4, A and B).

Illustrating the resemblance to human PVL is an MRI image of the brain of a 1-year-old child born prematurely, at gestational week 30, and diagnosed with PVL manifesting enlarged ventricles and reduced periventricular tissue, including the striatum (Supplemental Figure 4C).

Loss of periventricular vessels leads to a PVL-like phenotype: secondary lesions affecting late out-migrating neurons. Neuronal deficits in PVL encompass not only the periventricular zone, but also neurons that are more peripheral. It is assumed that the latter deficits develop secondarily to damage to the neurogenic niches of the GM and, correspondingly, that the neuronal subsets mostly affected are those born in and migrating out of this region during late gestation. We took advantage of our ability to inflict damage solely to the embryonic GE at a selected gestational time in order to follow consequences of early and late out-migrating neurons destined to the outer cortex. Of particular interest were GABAergic inhibitory

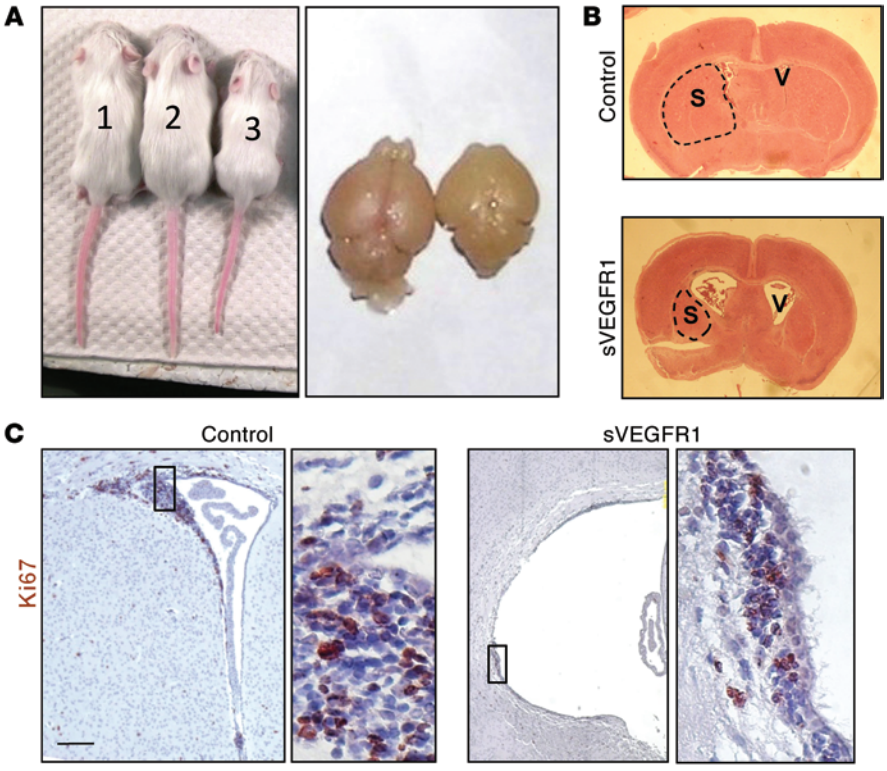

Figure 6. PVL-like pathology in sVEGFR1 mice. (**A**) 30-day-old littermates in which sVEGFR1 has been induced at E12.5. Note smaller size of the manipulated animal (left image, animal no. 3) and smaller brain size and missing olfactory bulb (right image, brain at the right). (**B**) H&E-stained sections of brains retrieved from mice shown in **A**. Note the enlarged lateral ventricles and reduced striatum (S, encircled by a dashed line) in the manipulated brain. Scale bar: 1 mm. (**C**) Ki-67 immunostaining (brown) of the SVZ area in a P30 littermate control (left) and the same area in sVEGFR1-manipulated brain (right). Scale bar: 200 μm. Images reproduced represent at least 15 animals.

interneurons originating at the embryonic GE and out-migrating in a sequential "inside-out" order, with interneurons born at E12.5 mostly populating cortical layers V–VI and interneurons born at E16.5 mostly populating layers II–III (23). Induction of sVEGFR1 at E12.5 (anticipating actual GE damage from E13.5 and onwards) led to gross underrepresentation of GABAergic inhibitory interneurons (highlighted by parvalbumin [PV] immunostaining) in superficial (II–III) cortical layers, whereas their presence in deeper cortical layers was unaffected, as indeed expected, considering that these layers were already populated before GE damage was inflicted (Figure 7A).

Unlike GABAergic inhibitory interneurons originating from the subpallial GE, coinhabiting excitatory pyramidal neurons originate from the DVZ (24), a region spared by our manipulation. To determine whether these neurons, composing the vast majority of cortical neurons, would be similarly affected by VEGF blockade, the same brains were stained for the panneuronal marker NeuN (Figure 7B). No significant change in the number of $NeuN^+$ cells could be detected, indicating that lamination of projection neurons was unaffected. Together, these findings indicate that the neuronal deficit is restricted only to GE-born neurons and only to those scheduled to out-migrate after GE damage occurred. Strengthening resemblance to the human condition, a decreased density of GABAergic neurons in VLBW premature infants with PVL has been reported (25, 26). A cortical deficit in GABAergic interneurons was also observed in baboons that were born prematurely and suffered from PVL-like symptoms (11). Our findings, therefore, not only attest that our experimental system reproduces a PVL-like deficit in GABAergic interneurons, but also reinforce the notion that this deficit represents a secondary outcome to periventricular vascular injury in the preterm neonate.

Discussion

We propose herein a unifying principle implicating the state of vessel immaturity at the time of immature birth as the key determinant defining both temporal and spatial patterns of vulnerability to neuronal injuries of prematurity. Specifically, we argue that those vessels at risk are only vessels that have remained immature at the time when the pathogenic insult is applied, and therefore, permanent neuronal damage is restricted to cerebral regions served by these vessels. This pathogenic mechanism may thus explain the restricted brain region affected as well as the closure of the vulnerability window. While this paradigm clearly applies for retinal vessels, it has not been previously addressed in the case of neuronal injuries affecting the immature brain. Here, we focus on PVL pathogenesis, not only because of its paramount clinical significance, but also because explaining its regional specificity is particularly challenging, considering that the primary cerebral damage is confined to the periventricular zone and the secondary, peripheral neuronal deficit involves particular neuronal subsets. Notably, the mechanism proposed herein is conceptually different from the notion that periventricular vessels are intrinsically unique and hence more sensitive than other cerebral vasculatures to insults, conceivably, to impaired oxygenation. A number of studies indeed ascribe PVL to regional hypoxia-ischemia but, again, it remained unclear why impaired oxygenation is restricted to the specific region affected.

Setting the stage for our proposed scenario are findings described above showing that maturation of cortical vessels takes place in a progressive, wave-like fashion, with periventricular vessels within the GM being the last vessels to mature. Vessel maturation was first defined by the timing of acquiring pericyte coverage and tight-junction molecule expression, both considered a prerequisite for consolidation of a functional BBB; refs. 17, 21). It is noteworthy that tight-junction expression is also relatively delayed in human GM vessels (27) (but also see ref. 28 reporting no difference in tight-junction expression) and that their pericyte coverage also lags behind that of other cerebral vessels (29). More indicative than marker expression, however, is the status of BBB functionality. We have provided what we believe is the first in situ mapping of BBB functional status during sequential stages of brain development, with results corroborating a delayed acquisition by

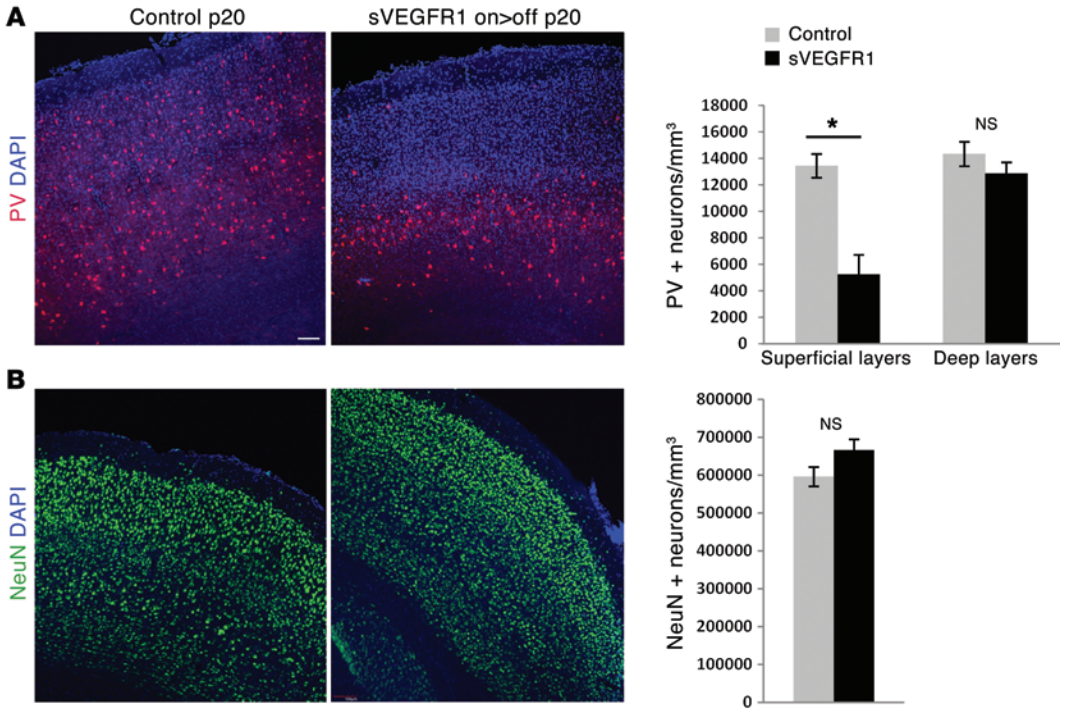

Figure 7. A deficit in cortical inhibitory GABAergic interneurons in sVEGFR1 mice. sVEGFR1 was induced from E12.5 to P1 and brains retrieved for analysis at P20. (**A**) GABAergic interneurons were highlighted by PV staining (red) and separately enumerated in superficial and deep cortical layers. (**B**) The entire neuronal population visualized by NeuN staining and similarly enumerated. Note a marked deficit in GABAergic interneurons, specifically in superficial cortical layers, but no significant difference in overall number of cortical neurons. $n = 4$ in each group. $^*P = 0.0028$, $t(6) = 4.801$. Scale bars: 100 μm.

periventricular vessels of a functional BBB and a gross correspondence between the gestational timing of these vessels acquiring a functional BBB and becoming refractory. Perhaps even more relevant for this study is the transition from a VEGF-dependent to a VEGF-refractory state. Using this operational parameter, we show that just before closure of the vulnerability window, VEGF blockade results in complete obliteration of exclusively GE vessels. The compete correspondence between vessel immaturity and vascular VEGF-dependence status resembles the situation in the retina in which VEGF suppression by high oxygen results in selective obliteration of immature retinal vessels, consequent regional hypoxia, and ROP. By way of extrapolation, it might be suggested that iatrogenic hyperoxia may represent a PVL-inducing insult leading to vessel regression, generation of vascular-free zones, and consequent regional ischemia/hypoxia. The proposition of a hyperoxia–VEGF suppression–vessel regression pathogenic axis is consistent with the fact that, similarly to ROP, in PVL, neuronal damage of subjects (all of them obligatorily spending a long time in oxygen chambers) develops in regions devoid of blood vessels (8). While our mouse model shows that GM avascularity enforced by VEGF blockade indeed triggers a PVL-like phenotype, a definite proof for this claim necessitates reproducing these phenotypes via direct exposure to oxygen during the vulnerable window of E14.5–E15.5 and rescue of the phenotype by exogenous VEGF, similar to the approach we previously used in elucidating the ROP paradigm (3). Unfortunately, however, it is technically impossible to sustain mouse embryos of this age ex vivo or efficiently hyperoxygenate them in utero. In support of this proposition, however, is a study showing that hyperoxygenation of prematurely delivered baboon neonates was sufficient to cause PVL-like damage to the periventricular area (10) and findings showing that pattern and magnitude of damage to GABAergic interneurons depend on the mode of ventilatory support applied (11).

Delineating primary events and secondary sequelae of this highly complex disease encompassing multiple cerebral regions has been hampered by the lack of an appropriate experimental system generating the highly restricted injury considered to be the primary lesion. Here, we harnessed a capability of inducing a no-perfusion zone exclusively in the relevant area of the GM to address this issue, as any neuronal damage occurring elsewhere necessarily represents a downstream consequence to this primary lesion rather than reflecting an unrelated occurrence. Thus, underrepresentation of GE-born GABAergic inhibitory interneurons in outer cortical layers in our system must be secondary to the massive periventricular apoptosis. By way of extrapolation, findings that in human PVL, periventricular necrosis is often accompanied by compromised development and/or migration of GABAergic inhibitory neurons destined to the overlying cortex suggest a similar hierarchy of events in the human condition.

Gross developmental and architectural differences between rodent and human brains likely account for the inability of our mouse model to accurately reproduce all phenotypes of human PVL, notably, limb motor deficits that develop in 5%–10% of human PVL cases, but were not reproduced in our mice (as judged from their performance in open-field exploration and the rotarod analyses [not shown]). This difference may reflect the fact that in PVL, neuronal damage is mainly to the corticospinal tract axons located near the GM, whereas in mice, these fibers are located lat-

erally to the striatum (30). Another difference concerns oligodendrocyte death, which is a major hallmark of human PVL; no significant reduction in oligodendrocyte numbers was observed in our system (data not shown). This is likely due to different anatomical distributions of oligodendrocytes that, in mice, are mostly located outside of the vulnerable GE and hence are spared (31) It was also shown that targeted ablation of GE-generated oligodendrocytes is compensated by oligodendrocytes generated elsewhere in the mouse brain (31). Likewise, differences in gestational out-migrating timing of periventricular-born neurons as well as differences in their periventricular subregions of origin are likely to determine which neuronal subset will be affected. For example, because the murine GE is essential for proper development of all telencephalic structures, it was not surprising that neuronal apoptosis in subpallial regions inflicted by vascular loss at E13.5 culminated in severe reduction of the striatum known to develop from these neurons (32). In human PVL, on the other hand, more lesions in the thalamus and fewer in the striatum are the common feature (33). Despite these interspecies differences, the general principle that periventricular necrosis due to vascular collapse adversely affects neuronal populations scheduled to out-migrate from the damaged area after injury is common to both species.

In summary, the study provides a mechanistic explanation for the gestation-stage–restricted vulnerability of human PVL and also explains the spatial pattern of incurred neuronal damage and provides missing insights into the nature of vascular injuries underlying PVL pathogenesis. Having mapped the distribution of immature vessels at the time of immature birth and equated the state of vessel immaturity with their absolute dependence on VEGF, we propose the following pathogenic scenario: cerebral hyperoxia associated with ventilator treatment of VLBW infants suppresses VEGF to below the level required to sustain immature vessels that are confined at the time of immature birth to the periventricular zone. Obliteration of periventricular vessels and a resultant massive periventricular necrosis then lead to a sequelae of destructive events affecting, among others, neuronal subsets originating at and out-migrating from the initially affected zone. While, unlike the ROP paradigm, which is done in the postnatal stage, the study comes short of providing a definite proof for a VEGF etiology in PVL, it provides a framework for its further pursuit. If substantiated, it may also have an impact on the management of VLBW infants similar to that of the recognition that hyperoxygenation represents an iatrogenic insult for ROP development.

Methods

Mice. Transgenic mouse lines used in this study were obtained as follows: the CamkIIα-tTA line was purchased from Jackson Laboratories (13); the Rosa26-rtTa driver was a gift of R. Jaenisch (Whitehead Institute, Massachusetts Institute of Technology, Cambridge, Massachusetts, USA) (34); the pTET-sVEGFR1 responder line was as described previously (35). Due to the use of multiple transgenic lines, we performed experiments on a C57/BL6-ICR cross-breed. For switching off I-sVEGFR1, water was supplemented with 500 mg/l tetracycline (Tevacycline, Teva Inc.) and 3% sucrose. For switching on the transgene, tetracycline-supplemented water was replaced by fresh water for the desired time. Pimonidazole (Hypoxyprobe, Chemicon, 60 mg/kg) was injected intraperitoneally 30 minutes prior to sacrifice. Regular specific pathogen–free housing conditions with a 12-hour light/12-hour dark cycle were used. Irradiated rodent food and water/tetracycline were given ad libitum. Both males and females were used for all experiments.

Immunohistochemistry. Formalin-fixed paraffin-embedded tissues were dissected to 3-μm sections. Staining was done as described (14) with the following: anti–human flt-1 (1:100, Abcam, no. Ab9450, or R&D, no. Af321), anti-Flk1 (1:200, Cell Signaling, no. 2479) Hypoxyprobe (1:100, Chemicon, no. 90204), Isolectin B4 (Ib4) (1:10, Sigma-Aldrich, no. L2140), anti–Ki-67 (1:200, Thermo Scientific, no. 9106), anti-NG2 (1:200, Chemicon, no. Ab3520), anti–claudin-5 (1:200 Zymed, no. 34-1600), anti–ZO-1 (1:200, Zymed, no. 61-7300), and anti–cleaved caspase-3 (1:200, Cell Signaling, no. 9961). Frozen sections were prepared by embedding the brain in 4% paraformaldehyde followed by 30% sucrose. 50-μm free-floating sections were stained with anti-PV (1:500, Abcam, no. Ab11427) and anti-NeuN (1:500, Cell Signaling, no. 12943). Cy5-conjugated extravidin, Cy2 anti-rabbit, Cy3 anti-mouse (Jackson), and ImmPRESS Universal (Vector, no. MP-7500) were used as secondary antibodies. Confocal microscopy was done using an Olympus FV-1000. Z-stacks were done on a ×10 air objective and at 2-μm intervals.

Embryonic BBB permeability assay. WT Swiss-Webster mice (Taconic Farms Inc.) were used. Deeply anesthetized pregnant mice were used, and a minimal volume of 10 kDa Dextran-Tetramethylrhodamine, Lysine Fixable (D1817, Invitrogen) or 500 kDa Dextran-FITC (Sigma-Aldrich FD-500S) was injected into the embryonic liver, while keeping the embryo connected to the maternal blood circulation through the umbilical cord (for E14.5, 2 μl; for E15.5, 3 μl; and for E16.5, 4 μl). After 5 minutes of tracer circulation, embryonic heads were fixed by immersion in 4% PFA overnight at 4°C, cryopreserved in 30% sucrose, and frozen in TissueTek OCT (Sakura). 12-μm sections were then collected and post-fixed in 4% PFA at room temperature for 15 minutes, washed in PBS, and costained with IB4 or CD31 to visualize blood vessels and with DAPI to visualize nuclei. Images were processed using Adobe Photoshop and ImageJ (http://imagej.nih.gov/ij/).

Statistics. $n \geq 4$ in all experimental groups. At least 4 images were taken for each animal, and analysis was done using the average value per animal. Experiments were successfully repeated in at least 3 independent litters, although the different experiments were not grouped for statistics. Image morphometry was performed blind to the experimental conditions. All values are shown as mean ± SEM. Student's *t* test was done using Excel (Microsoft) and SPSS (IBM) to compare between 2 groups using 1-tailed distribution and unequal variances. Normal distribution was assessed.

Study approval. All animal studies performed at the Hebrew University were approved by the Animal Care and Use Committee of the Hebrew University. Animal studies performed at Harvard University were approved by the IACUC of Harvard Medical School.

Acknowledgments

The study was supported by an advanced research grant from the European Research Council (ERC) (Project VASNICHE).

Address correspondence to: Eli Keshet, Department of Developmental Biology and Cancer Research, the Hebrew University Medical School, Jerusalem 91120, Israel. Phone: 972.2.6758496; E-mail: Keshet@cc.huji.ac.il.

1. Volpe JJ. Cerebral white matter injury of the premature infant-more common than you think. *Pediatrics*. 2003;112(1):176–180.
2. Smith LE, et al. Oxygen-induced retinopathy in the mouse. *Invest Ophthalmol Vis Sci*. 1994;35(1):101–111.
3. Alon T, Hemo I, Itin A, Pe'er J, Stone J, Keshet E. Vascular endothelial growth factor acts as a survival factor for newly formed retinal vessels and has implications for retinopathy of prematurity. *Nat Med*. 1995;1(10):1024–1028.
4. Volpe JJ. Brain injury in the premature infant. Neuropathology, clinical aspects, pathogenesis, and prevention. *Clin Perinatol*. 1997;24(3):567–587.
5. Leviton A, et al. Maternal infection, fetal inflammatory response, and brain damage in very low birth weight infants. Developmental Epidemiology Network Investigators. *Pediatr Res*. 1999;46(5):566–575.
6. Yoon BH, Park CW, Chaiworapongsa T. Intrauterine infection and the development of cerebral palsy. *BJOG*. 2003;110(suppl 20):124–127.
7. Leviton A, Dammann O, Durum SK. The adaptive immune response in neonatal cerebral white matter damage. *Ann Neurol*. 2005;58(6):821–828.
8. Takashima S, Tanaka K. Development of cerebrovascular architecture and its relationship to periventricular leukomalacia. *Arch Neurol*. 1978;35(1):11–16.
9. Ballabh P, Braun A, Nedergaard M. Anatomic analysis of blood vessels in germinal matrix, cerebral cortex, and white matter in developing infants. *Pediatr Res*. 2004;56(1):117–124.
10. Loeliger M, et al. Cerebral outcomes in a preterm baboon model of early versus delayed nasal continuous positive airway pressure. *Pediatrics*. 2006;118(4):1640–1653.
11. Verney C, Rees S, Biran V, Thompson M, Inder T, Gressens P. Neuronal damage in the preterm baboon: impact of the mode of ventilatory support. *J Neuropathol Exp Neurol*. 2010;69(5):473–482.
12. May D, et al. Transgenic system for conditional induction and rescue of chronic myocardial hibernation provides insights into genomic programs of hibernation. *Proc Natl Acad Sci U S A*. 2008;105(1):282–287.
13. Mayford M, Bach ME, Huang YY, Wang L, Hawkins RD, Kandel ER. Control of memory formation through regulated expression of a CaMKII transgene. *Science*. 1996;274(5293):1678–1683.
14. Licht T, Eavri R, Goshen I, Shlomai Y, Mizrahi A, Keshet E. VEGF is required for dendritogenesis of newly born olfactory bulb interneurons. *Development*. 2010;137(2):261–271.
15. Cao L, et al. VEGF links hippocampal activity with neurogenesis, learning and memory. *Nat Genet*. 2004;36(8):827–835.
16. Haigh JJ, et al. Cortical and retinal defects caused by dosage-dependent reductions in VEGF-A paracrine signaling. *Dev Biol*. 2003;262(2):225–241.
17. Benjamin LE, Hemo I, Keshet E. A plasticity window for blood vessel remodelling is defined by pericyte coverage of the preformed endothelial network and is regulated by PDGF-B and VEGF. *Development*. 1998;125(9):1591–1598.
18. Daneman R, Zhou L, Kebede AA, Barres BA. Pericytes are required for blood-brain barrier integrity during embryogenesis. *Nature*. 2010;468(7323):562–566.
19. Armulik A, et al. Pericytes regulate the blood-brain barrier. *Nature*. 2010;468(7323):557–561.
20. Liebner S, Czupalla CJ, Wolburg H. Current concepts of blood-brain barrier development. *Int J Dev Biol*. 2011;55(4):467–476.
21. Nitta T, et al. Size-selective loosening of the blood-brain barrier in claudin-5-deficient mice. *J Cell Biol*. 2003;161(3):653–660.
22. Ben-Zvi A, et al. Mfsd2a is critical for the formation and function of the blood-brain barrier. *Nature*. 2014;509(7501):507–511.
23. Miyoshi G, Fishell G. GABAergic interneuron lineages selectively sort into specific cortical layers during early postnatal development. *Cereb Cortex*. 2011;21(4):845–852.
24. Anderson SA, Kaznowski CE, Horn C, Rubenstein JL, McConnell SK. Distinct origins of neocortical projection neurons and interneurons in vivo. *Cereb Cortex*. 2002;12(7):702–709.
25. Vry J, et al. Altered cortical inhibitory function in children with spastic diplegia: a TMS study. *Exp Brain Res*. 2008;186(4):611–618.
26. Robinson S, Li Q, Dechant A, Cohen ML. Neonatal loss of gamma-aminobutyric acid pathway expression after human perinatal brain injury. *J Neurosurg*. 2006;104(6):396–408.
27. Anstrom JA, Thore CR, Moody DM, Brown WR. Immunolocalization of tight junction proteins in blood vessels in human germinal matrix and cortex. *Histochem Cell Biol*. 2007;127(2):205–213.
28. Ballabh P, Hu F, Kumarasiri M, Braun A, Nedergaard M. Development of tight junction molecules in blood vessels of germinal matrix, cerebral cortex, and white matter. *Pediatr Res*. 2005;58(4):791–798.
29. Braun A, et al. Paucity of pericytes in germinal matrix vasculature of premature infants. *J Neurosci*. 2007;27(44):12012–12024.
30. Canty AJ, Murphy M. Molecular mechanisms of axon guidance in the developing corticospinal tract. *Prog Neurobiol*. 2008;85(2):214–235.
31. Kessaris N, Fogarty M, Iannarelli P, Grist M, Wegner M, Richardson WD. Competing waves of oligodendrocytes in the forebrain and postnatal elimination of an embryonic lineage. *Nat Neurosci*. 2006;9(2):173–179.
32. Evans AE, Kelly CM, Precious SV, Rosser AE. Molecular regulation of striatal development: a review. *Anat Res Int*. 2012;2012:106529.
33. Volpe JJ. Brain injury in premature infants: a complex amalgam of destructive and developmental disturbances. *Lancet Neurol*. 2009;8(1):110–124.
34. Beard C, Hochedlinger K, Plath K, Wutz A, Jaenisch R. Efficient method to generate single-copy transgenic mice by site-specific integration in embryonic stem cells. *Genesis*. 2006;44(1):23–28.
35. Licht T, et al. Reversible modulations of neuronal plasticity by VEGF. *Proc Natl Acad Sci U S A*. 2011;108(12):5081–5086.